



Seismic design guidelines for solid and perforated hybrid precast concrete shear walls

Brian J. Smith and Yahya C. Kurama

- This paper presents recommended seismic design and detailing guidelines for special unbonded posttensioned hybrid precast concrete shear walls.
- Hybrid precast concrete walls use a combination of mild steel bars and high-strength unbonded posttensioning steel strands for lateral resistance across horizontal joints.
- The proposed design guidelines support the U.S. code approval of the hybrid precast concrete wall system as a special reinforced concrete shear wall for moderate and high seismic regions.

The hybrid precast concrete wall system investigated in this paper (**Fig. 1**) was constructed by placing rectangular precast concrete panels across horizontal joints at the foundation and floor levels.¹⁻⁴ The term *hybrid* reflects that a combination of Grade 400 (Grade 60) mild steel bars and high-strength unbonded posttensioning strands was used for the lateral resistance of the structure across the critical joint between the base panel and the foundation (that is, the base joint). Under the application of lateral loads into the nonlinear range, the primary mode of displacement in a well-designed hybrid precast concrete shear wall occurs through a gap at the base joint, allowing the wall to undergo large nonlinear lateral displacements with little damage. On unloading, the posttensioning steel provides a vertical restoring force (in addition to the gravity loads acting on the wall) to close this gap, thus significantly reducing the residual lateral displacements of the structure after a large earthquake. The use of unbonded tendons delays the yielding of the posttensioning strands and reduces the tensile stresses transferred to the concrete (thus reducing cracking) as the tendons elongate under lateral loading. The mild steel bars across the base joint are designed to yield in tension and compression and provide energy dissipation through the gap opening and closing behavior of the wall under reversed-cyclic lateral loading. A predetermined length of these energy-dissipating bars is unbonded at the base joint (by wrapping the bars with plas-

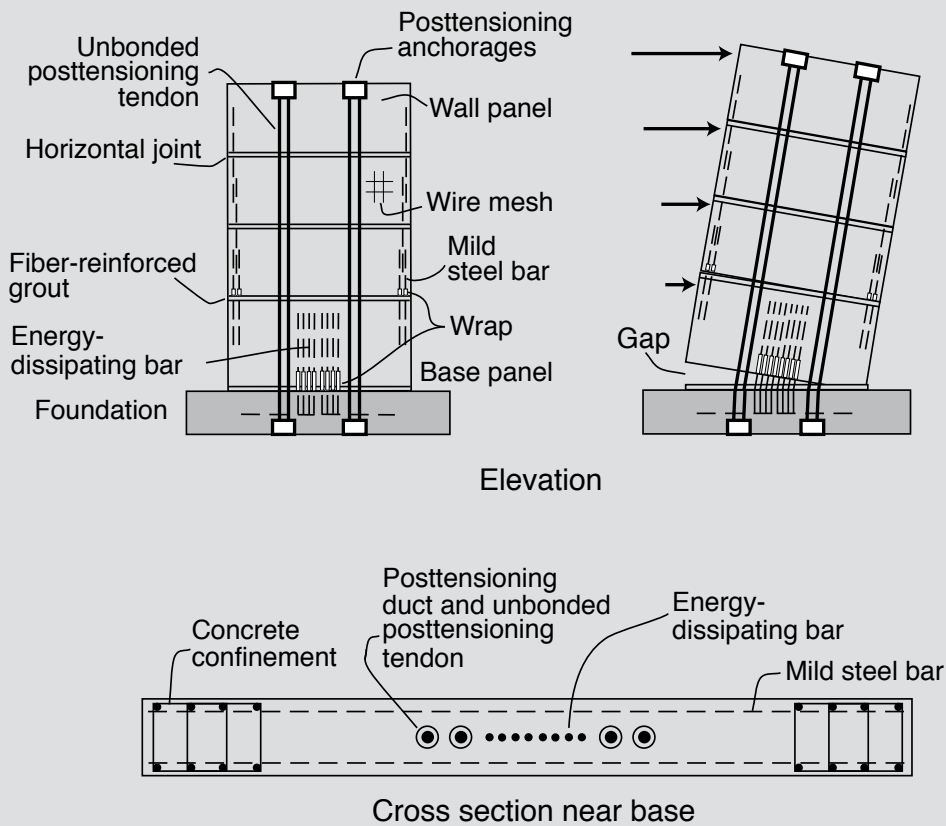


Figure 1. Elevation, exaggerated displaced position, and cross section of a hybrid wall.

tic sleeves) to limit the steel strains and prevent low-cycle fatigue fracture.

Hybrid precast concrete shear walls are efficient structures that offer high-quality production, relatively simple erection, and excellent seismic characteristics by providing self-centering to restore the building toward its original undisplaced position as well as energy dissipation to limit lateral displacement during an earthquake. Despite these desirable characteristics, hybrid precast concrete walls are classified as nonemulative structures because their behavior under lateral loads is different from that of conventional monolithic cast-in-place reinforced concrete shear walls. Thus, experimental validation is required by the American Concrete Institute's (ACI's) *Building Code Requirements for Structural Concrete and Commentary (ACI 318-11)*⁵ and *Acceptance Criteria for Special Unbonded Post-Tensioned Precast Structural Walls Based on Validation Testing and Commentary (ACI ITG-5.1)*⁶ prior to the use of these structures in seismic regions of the United States.

Research objectives and significance

The primary objective of the research described in this paper is to advance precast concrete building construction by conducting the required experimental validation and

associated design and analytical studies for code approval of hybrid wall structures as *special* reinforced concrete shear walls per Chapter 21 of ACI 318-11. The project provides new information in accordance with and directly addressing the ACI ITG-5.1 validation requirements as well as information regarding the behavior of hybrid precast concrete walls featuring multiple wall panels (that is, multiple horizontal joints over the wall height) and panel perforations, both common features in practical building construction. The experimental results demonstrate that hybrid precast concrete walls can satisfy all requirements for special reinforced concrete shear walls in high seismic regions with improved performance, while also revealing important design, detailing, and analysis considerations to prevent undesirable failure mechanisms. It is not the objective of this paper to provide full details on the experiments, which can be found elsewhere.¹⁻⁴ Instead, only the relevant experimental results that support the proposed design recommendations are provided.

Overview of proposed design guidelines

The design, detailing, and analysis guidelines and recommendations provided in this paper are intended for use by practicing engineers and precast concrete producers involved in the design of hybrid shear walls in moderate

and high seismic regions. Where appropriate, ACI 318-11 requirements for special monolithic cast-in-place reinforced concrete shear walls are used to help in the adoption of the recommended guidelines. Furthermore, applicable references and suggested modifications and additions to the design recommendations in *Requirements for Design of a Special Unbonded Post-Tensioned Precast Shear Wall Satisfying ACI ITG-5.1 and Commentary (ACI ITG-5.2)*⁷ are given. The recommendations developed by this project include a performance-based design procedure and a prescriptive design procedure.¹ This paper summarizes key guidelines from the performance-based design procedure. A detailed example demonstrating step-by-step application of the design procedure, including recommended capacity reduction factors, can be found online in the appendix at http://www.pci.org/Publications/PCI_Journal/2014/Summer/.

The proposed guidelines can be used to design hybrid walls with height-to-length H_w/L_w aspect ratios of at least 0.5 in low- to mid-rise structures with a practical height limitation of 36.5 m (120 ft), or approximately eight to ten stories. The procedure is applicable to both single-panel wall systems (featuring only the base joint) as well as multi-panel systems (featuring base panel-to-foundation and upper panel-to-panel joints) with or without panel perforations. The design is conducted at two wall drift values: the wall drift corresponding to the design-basis earthquake (DBE) Δ_{wd} and the wall drift corresponding to the maximum-considered earthquake (MCE) Δ_{wm} . The wall drift Δ_w is defined as the lateral displacement of the wall at the roof level with respect to the foundation divided by the wall height from the top of the foundation H_w . While all lateral deformations and rotations of the wall due to flexure, shear, and horizontal shear slip are included in the calculation for Δ_w ,⁶ shear slip across the horizontal joints and gap opening across the upper panel-to-panel joints can be ignored because the design of a wall includes provisions to prevent these undesirable deformation behaviors.

Figure 2 shows the idealized base shear force versus roof drift behavior of a properly designed hybrid precast concrete wall subjected to these drift demands. The corresponding expected wall performance at Δ_{wd} is as follows:

- gap opening at the base joint but no gap opening or nonlinear material behavior at the upper panel-to-panel joints
- no residual vertical uplift of the wall upon removal of lateral loads (that is, the gap at the base joint fully closes upon unloading)
- no shear slip at the horizontal joints
- yielding of the energy-dissipating bars

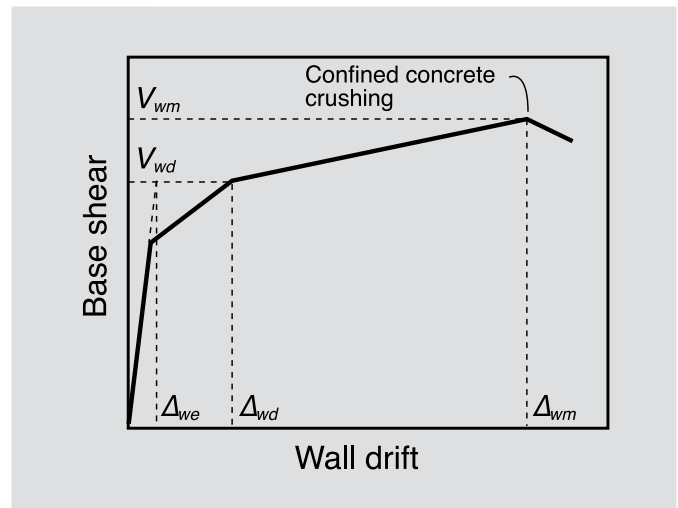


Figure 2. Idealized base shear force versus roof drift behavior. Note: V_{wd} = design wall base shear force at Δ_{wd} ; V_{wm} = maximum wall base shear force at Δ_{wm} ; Δ_{wd} = design-level wall drift corresponding to design-basis earthquake; Δ_{we} = linear-elastic wall drift under design base shear force V_{wd} ; Δ_{wm} = maximum-level wall drift corresponding to maximum considered earthquake.

- posttensioning steel remaining in the linear-elastic range
- minor hairline cracking in the base panel (for perforated walls, cracking may extend into the upper panels)
- no observable concrete damage in compression but cover concrete at the wall toes on the verge of spalling

The corresponding expected wall performance at Δ_{wm} is as follows:

- increased gap opening at the base joint but no significant gap opening or nonlinear material behavior at the upper panel-to-panel joints
- no significant residual vertical uplift of the wall upon removal of lateral loads
- no significant shear slip at the horizontal joints
- significant yielding but no fracture of the energy-dissipating bars
- posttensioning steel in the nonlinear range but with strains not exceeding 0.01
- well distributed, still hairline, cracking of the concrete (limited to the base panel in solid walls)
- cover concrete spalling at the wall toes, with the confined core concrete on the verge of crushing

The proposed design guidelines to achieve these performance objectives were validated using the measured and predicted behaviors of six 0.4-scale wall test specimens (four solid and two perforated walls) subjected to service-



Table 1. Selected specimen properties: Part 1

Specimen	κ_d		Posttensioning tendons			Energy-dissipating bars					Total gravity load at base, kN*
	Design	Actual	Number of 12.7 mm diameter strands	f_{pi}/f_{pu}	Eccentricity e_p , mm	Size	Eccentricity e_s , mm	Wrapped length, mm	$\epsilon_{sm}/\epsilon_{su}$	Detail at base	
HW1	0.50	0.53	3	0.54	±229	19M	±76, 152	254	0.64	Spliced	361
HW2	0.50	0.53	3	0.54	±229	19M	±76, 152	254	0.61	Spliced	361
HW3	0.50	0.50	3	0.54	±279	19M	±89, 191	381	0.48	Continuous	361
HW4	0.50	0.54	3	0.54	±279	19M	±89, 191	381	0.49	Continuous	361
HW5	0.85	0.90	2	0.54	±140	22M	±229, 864	254, 406	0.85	Continuous	534
EW	n/a	n/a	n/a	n/a	n/a	22M	±788, 914, 1041	559	0.73	Spliced	361

* Total gravity load includes wall self-weight and externally applied gravity load.

Note: e_p = distance of tension-side and compression-side posttensioning tendons from wall centerline; e_s = distance of tension-side and compression-side energy-dissipating bars from wall centerline; f_{pi} = average initial strand stress; f_{pu} = design ultimate strength of strand = 1862 MPa; n/a = not applicable; ϵ_{sm} = expected (design) energy-dissipating bar strain at maximum-level wall drift $\Delta_{wm} = 2.30\%$; ϵ_{su} = strain at maximum (peak) strength of energy-dissipating bar from monotonic material testing; κ_d = energy-dissipating steel moment ratio, defining relative amounts of energy-dissipating resistance (from energy-dissipating steel) and restoring resistance (from posttensioning steel and gravity axial force) at wall base. 1 mm = 0.0394 in.; 1 kN = 0.225 kip; 1 MPa = 0.145 ksi.

level gravity loads combined with quasi-static reversed-cyclic lateral loads satisfying ACI ITG-5.1.²⁻⁴ **Tables 1 and 2** provide some of the important features of these wall specimens. Specimens HW1 through HW5 were hybrid walls, and specimen EW was an emulative precast concrete wall with no posttensioning steel reinforcement (that is, the entire lateral resistance of the wall was provided by mild steel bars).³ While outside the scope of this paper, three analytical models were developed by this project¹ as experimentally-validated tools for engineers to design hybrid walls with predictable and reliable behavior under

lateral loads. The recommendations for a linear-elastic effective stiffness model (which can be used to estimate the linear-elastic lateral displacement demands) and a nonlinear finite element model (used to conduct nonlinear monotonic lateral load analyses and aid in the design of hybrid walls with perforations) intentionally incorporate several simplifying assumptions appropriate for the design office. Recommendations for a detailed fiber element model (used to conduct nonlinear reversed-cyclic lateral load analyses and dynamic analyses) were also developed.³

Table 2. Selected specimen properties: Part 2

Specimen	Panel perforations, mm	Confined region details				Distributed panel reinforcement	
		l_m , mm	l_{hoop} , mm	s_{hoop} , mm	s_{dot} , mm	Type	End Detail
HW1	n/a	406	406	83	114	Welded wire fabric	Developed outside confined region
HW2	n/a	406	406	83	19	10M	Developed outside confined region
HW3	n/a	406	406	76	19	10M	Developed outside confined region
HW4	356 × 508	470	254	64	19	10M	Developed inside confined region
HW5	456 × 508	470	254	64	19	10M	Developed inside confined region
EW	n/a	203	203	83	19	10M	Developed outside confined region

Note: l_m = confined region length at wall toes (center-to-center of hoop bars); l_{hoop} = length of individual confinement hoop (center-to-center of hoop bars); n/a = not applicable; s_{dot} = first hoop distance from bottom of base panel to center of hoop bar; s_{hoop} = confinement hoop spacing (center-to-center of hoop bars). 1 mm = 0.0394 in.



Determination of seismic forces and drift demands

The design of a hybrid wall should be conducted under all applicable load combinations prescribed by *Minimum Design Loads for Buildings and Other Structures (ASCE/SEI 7-10)*,⁸ including the use of a redundancy factor and torsional effects from accidental and applied eccentricities. The design base shear force can be obtained using any of the procedures allowed in ASCE 7-10, such as the equivalent lateral force procedure or the modal analysis procedure. The most basic approach is the equivalent lateral force procedure (appendix design example), in which the wall design base shear force V_{wd} is determined by dividing the first mode linear-elastic force demand under the DBE with the prescribed response modification factor R . When selecting R using Table 12.2-1 in ASCE 7-10, the seismic force-resisting system for hybrid walls can be classified as special reinforced concrete shear walls. Therefore, the response modification factors R should be taken as 5.0 and 6.0 for bearing wall systems and building frame systems, respectively. Once the design base shear force V_{wd} is established, the design base moment M_{wd} can be found from a linear-elastic analysis of the structure under the vertical distribution of the design base shear force from ASCE 7-10.

Appropriate analytical techniques, such as nonlinear dynamic response history analyses under properly selected DBE and MCE ground motion sets, can be used to determine the design-level drift Δ_{wd} and the maximum-level drift Δ_{wm} . Alternatively, the ASCE 7-10 guidelines in section 12.8.6 can be used to determine Δ_{wd} by multiplying the linear-elastic wall drift Δ_{we} under the design base shear force V_{wd} with the prescribed deflection amplification factor C_d . When selecting C_d from Table 12.2-1 in ASCE 7-10, the seismic force-resisting system for hybrid walls should be classified as special reinforced concrete shear walls, resulting in C_d equal to 5.0. The linear-elastic wall drift Δ_{we} (flexural plus shear displacements corresponding to V_{wd}) can be calculated using an effective linear-elastic stiffness model. As described in Smith and Kurama,¹ for design purposes the linear-elastic effective flexural and shear stiffnesses can be determined using an effective moment of inertia I_e and effective shear area A_{sh} , respectively, as given in Eq. (1) and (2).

$$I_e = 0.50I_{gross} \quad (1)$$

where

I_{gross} = moment of inertia of gross wall cross section

$$A_{sh} = 0.80A_{gross} \quad (2)$$

where

A_{gross} = area of gross wall cross section

For perforated walls, I_{gross} should be taken at the cross section of the base panel including the perforations. The shear deformations are considerably increased due to the presence of panel perforations; and thus, the effective shear area A_{sh} should be taken as the gross cross-sectional area of only the exterior vertical chord on the compression side of the base panel (that is, the compression vertical chord located outside of the perforations) without the 0.8 factor in Eq. (2). The other vertical chords located on the tension side of the wall and in between perforations do not contribute significantly to the shear stiffness; thus they should not be included in the effective shear area.

Unless nonlinear dynamic response history analyses are conducted under properly selected MCE ground motion sets, the maximum-level wall drift Δ_{wm} can be estimated from approximate methods that consider the unique hysteretic characteristics of hybrid precast concrete walls (in particular, the reduced energy dissipation and increased self-centering).^{9,10} For the test specimens in this project, Δ_{wm} was taken equal to the prescribed validation-level wall drift Δ_{wc} in ACI ITG-5.1 given as Eq. (3).

$$\Delta_{wc} = 0.9\% \leq \frac{H_w}{L_w} 0.8\% + 0.5\% \leq 3.0\% \quad (3)$$

For the full-scale wall dimensions of H_w equal to 13.7 m (45.0 ft) and L_w equal to 6.1 m (20.0 ft), the validation-level wall drift Δ_{wc} was 2.30%, and this value was used as Δ_{wm} in the design of the test specimens. The validity of using Δ_{wm} equal to 2.30% for design was supported by nonlinear dynamic response history analyses of the prototype structures under selected sets of MCE ground motion records.^{11,12}

Design of base joint

The design for the base joint of a hybrid precast concrete wall includes the determination of the energy-dissipating and posttensioning steel areas, probable (maximum) base moment strength of the wall, contact length (neutral axis length) and confinement reinforcement at the wall toes, energy-dissipating steel strains and stresses (including the determination of the unbonded length for the energy-dissipating bars), and posttensioning steel strains and stresses (including the determination of the posttensioning steel stress losses).

Reinforcement crossing base joint

The posttensioning and energy-dissipating steel areas crossing the base joint can be determined¹ using fundamental concepts of reinforced and prestressed concrete mechanics (equilibrium, compatibility and kinematics, and design constitutive relationships). As demonstrated in the

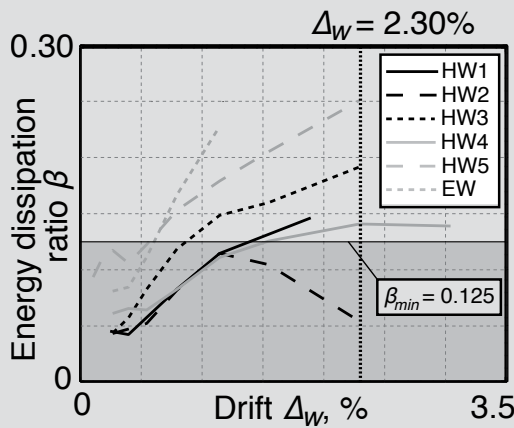


Figure 3. Energy dissipation ratio. Note: β_{min} = minimum required relative energy dissipation ratio per ACI ITG-5.1.

design example, a key parameter selected by the designer during this process is the energy-dissipating steel moment ratio κ_d , which is defined in Eq. (4).

$$\kappa_d = \frac{M_{ws}}{M_{wp} + M_{wn}} \quad (4)$$

where

M_{wn} = contribution of wall design gravity axial force N_{wd} to satisfy M_{wd}

M_{wp} = contribution of posttensioning steel to satisfy M_{wd}

M_{ws} = contribution of energy-dissipating steel to satisfy M_{wd}

The κ_d ratio is a relative measure of the resisting moments from the energy-dissipating force provided by the energy-dissipating steel reinforcement and the restoring (that is, self-centering) force provided by the posttensioning steel reinforcement plus the gravity axial load in the wall.¹³ If κ_d is too small, the energy dissipation of the structure may be small. Conversely, if κ_d is too large, the self-centering capability of the wall may not be sufficient to yield the tensile energy-dissipating bars back in compression and close the gap at the base joint on removal of the lateral loads. The κ_d values used in the design of the test specimens in this project ranged from 0.50 to 0.85, with the actual κ_d values for the as-tested structures (using the provided steel areas) ranging from 0.50 to 0.90 (Table 1).

Based on the performance of the test specimens,²⁻⁴ the κ_d value used in design should not exceed 0.80 to ensure sufficient self-centering and should not be less than 0.50 to ensure sufficient energy dissipation. Specimens with κ_d values close to both of these limits were tested. **Figure 3** shows the relative energy dissipation ratio β

(as defined in ACI ITG-5.1) of the six specimens as a function of wall drift. Specimen HW4, with design κ_d equal to 0.50 and actual κ_d equal to 0.54, satisfied the minimum relative energy dissipation ratio β_{min} of 0.125 prescribed by ACI ITG-5.1 with a small margin, leading to the recommended lower limit of κ_d equal to 0.50 for design. Specimen HW4 was a perforated wall, which increased the shear deformations in the wall panels, resulting in reduced energy dissipation. Although it may be possible to use a reduced value for the lower κ_d limit for solid hybrid walls, this was not investigated by this research project.

The recommended upper limit of κ_d equal to 0.80 was selected based on the premature failure of specimen HW5 (with design κ_d equal to 0.85 and actual κ_d equal to 0.90) before sustaining three loading cycles at the ACI ITG-5.1 validation drift Δ_{wc} of 2.30%. This specimen suffered from a loss of restoring force and failed due to the permanent uplift of the wall from the foundation (that is, a gap formed along the entire base joint when the wall was unloaded to Δ_w of 0%), which resulted in the subsequent out-of-plane displacements of the wall base and buckling of the energy-dissipating bars in compression. Wall uplift and excessive out-of-plane displacements (or in-plane slip as was observed in the emulative specimen EW)¹ resulting from loss or lack of restoring force across the base joint can develop quickly and lead to failure. **Figure 4** shows the measured base shear force V_b versus wall drift Δ_w behavior of specimen HW5, where the loss of restoring force can be seen by the unloading curves that do not return through the origin. The observed out-of-plane displacements and buckling of the energy-dissipating bars at the base joint are also shown. The goal of the recommended upper limit on κ_d is to prevent this type of behavior.

Confinement reinforcement at wall toes

Confinement reinforcement, composed of closely-spaced closed hoops, is required at the bottom corners (called toes) of the base panel to prevent premature crushing and failure of the core (inner) concrete prior to the maximum-level wall drift Δ_{wm} . The confinement steel ratio, hoop layout, and hoop spacing can be designed according to sections 5.6.3.5 through 5.6.3.9 in ACI ITG-5.2 (appendix design example). Based on the extent of the cover concrete spalling in the test specimens and accurate measurement of the concrete compression strains using digital image correlation,²⁻⁴ the confined concrete region at the wall toes should extend vertically over a height of the base panel not less than the plastic hinge height h_p , defined as $0.06H_w$ per ACI ITG-5.2. **Figure 5** shows the north toe of the base panel in specimens HW3 and HW4 (where h_p equals 330 mm [13 in.] for each wall) at the conclusion of each test. The observed vertical extent of cover spalling in specimens HW3 and HW4 was approximately 356 (14.0)

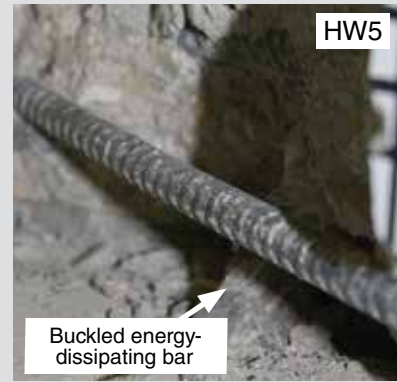
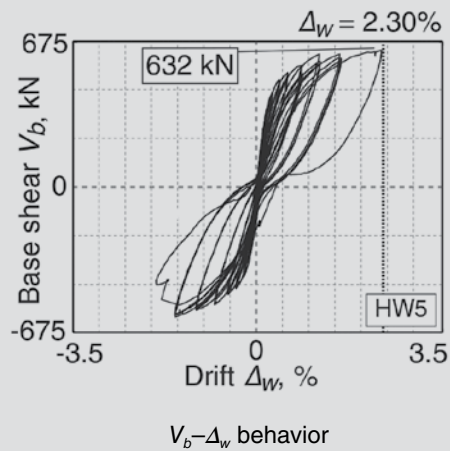


Figure 4. Performance of specimen HW5. Note: 1 kN = 0.225 kip.

and 305 mm (12.0 in.), respectively, supporting the design recommendation. Because the specimen length and height were not varied in this experimental program, additional research may be needed to validate the plastic hinge height recommendation in ACI ITG-5.2 for walls of different size. As required by ACI ITG-5.2, the confined region should extend horizontally from each end of the base panel over a distance not less than $0.95c_m$ and not less than 305 mm, where c_m is the neutral axis length¹ (contact length) at the wall base when Δ_{wm} is reached.

The design and detailing of the confinement reinforcement should satisfy all applicable requirements for special boundary regions as well as the requirements for bar spacing and concrete cover in ACI 318-11. The distance of the first confinement hoop from the base of the wall is critical to the performance of the confined concrete. The first hoop should be placed at a distance from the bottom of the base panel no greater than the minimum required concrete cover

per ACI 318-11. This recommendation was not satisfied in specimen HW1 (Table 2) due to the accidental slanted placement of the hoops during fabrication of the base panel, resulting in premature confined concrete crushing (**Fig. 6**).

The length-to-width aspect ratio (measured center-to-center of bar) for rectangular hoops should not exceed 2.50. This requirement is slightly more conservative than but similar to the requirements in past seismic design code specifications for concrete confinement (for example, section 1921.6.6.6 of the 1997 *Uniform Building Code, Volume 2: Structural Engineering Design Provisions*),¹⁴ which have since been removed from codes in the United States. As observed from the performance of the wall toes in specimen HW3 (**Fig. 6**), a large length-to-width ratio for the hoops can permit bowing of the longer hoop legs in the out-of-plane direction, reducing the confinement effectiveness. Further, intermediate crossies were ineffective



Figure 5. Performance of base panel north toe. Note: 1 mm = 0.0394 in.

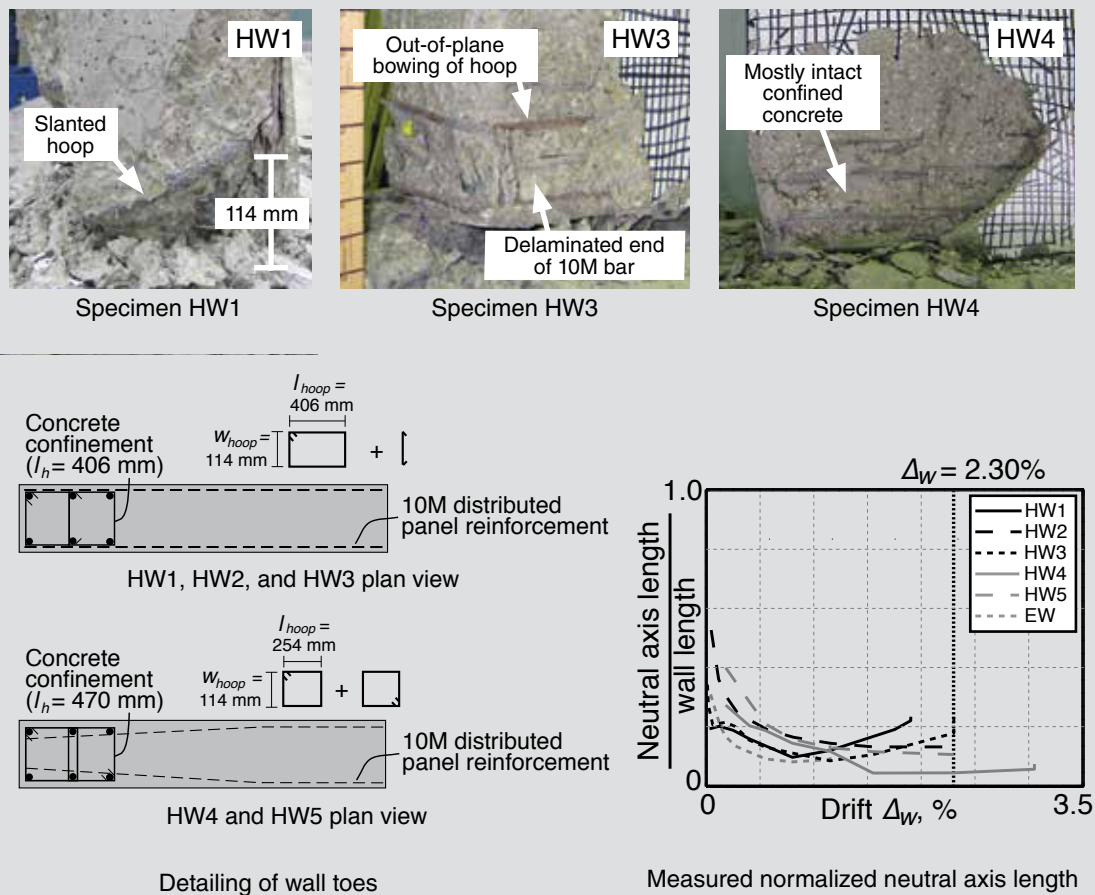


Figure 6. Performance and detailing of wall toes. Note: l_h = confined region length (center to center of bars); l_{hoop} = length of individual confinement hoop (center to center of bars); w_{hoop} = width of individual confinement hoop (center-to-center of bars). 10M = no. 3. 1 mm = 0.0394 in.

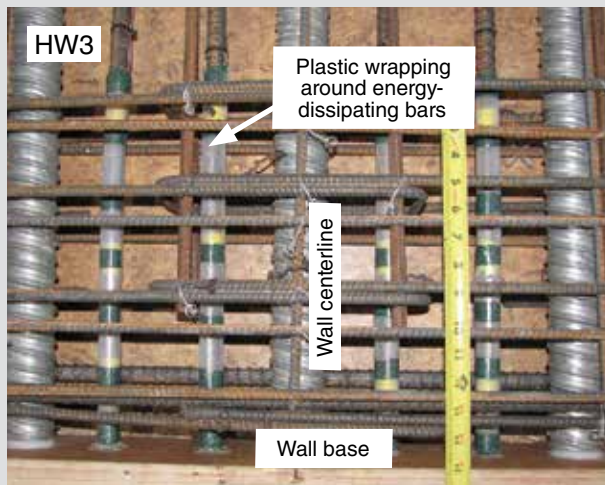
in preventing the outward bowing of the longer hoop legs because in typical construction the cross-ties do not directly engage the hoop steel. (Rather, the cross-ties engage the vertical reinforcement within the hoops.) For comparison, specimens HW4 and HW5 followed all of the hoop design and detailing recommendations made herein, resulting in excellent behavior of the confined concrete at the wall toes.³ Figure 6 shows the performance of specimen HW4 and the confinement detailing differences between the hybrid wall specimens.

Figure 6 further demonstrates the confined concrete performance with plots of the measured neutral axis length across the base joint at the south end of the walls. The results are shown for the peak of the first cycle in each drift series, except for the last series where the peaks from all three cycles are shown. During the small displacements of each wall, the neutral axis length went through a rapid decrease associated with gap opening at the base. As each wall was displaced further, the neutral axis length continued to decrease but at a much slower pace. Once deterioration of the confined concrete at the wall toes initiated, the neutral axis began to lengthen to satisfy equilibrium with the reduced concrete stresses. This effect was more evident during the final drift series for specimens HW1 and HW3, and was es-

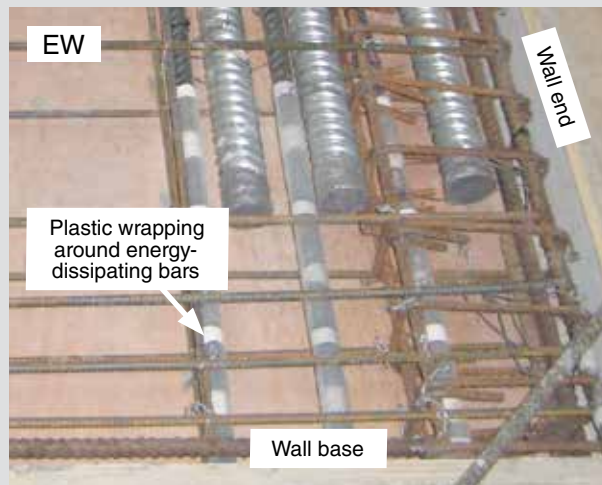
pecially exacerbated due to the premature crushing of the confined concrete in specimen HW1. In specimens HW4 and HW5, the neutral axis remained stable over a much larger drift range as the lengthening of the neutral axis was not observed in specimen HW5 and was evident in specimen HW4 only after achieving the validation-level drift Δ_{wc} of 2.30%. This was primarily due to the confinement steel detailing improvements incorporated into these specimens (Fig. 6).

Energy-dissipating bar strains and unbonded length

The performance-based seismic design of a hybrid precast concrete shear wall requires an iterative process where the energy-dissipating bar strains are estimated based on a predicted neutral axis length. As demonstrated in the appendix design example, the elongations of the energy-dissipating bars can be found by assuming that the wall displaces like a rigid body rotating through the gap opening at the base joint.¹ The strain in each bar can then be calculated by dividing the bar elongation with the total unbonded length, which is taken as the sum of the plastic-wrapped length and an additional length of debonding that is expected to develop during the reversed-cyclic lateral displacements



Specimen HW3



Specimen EW

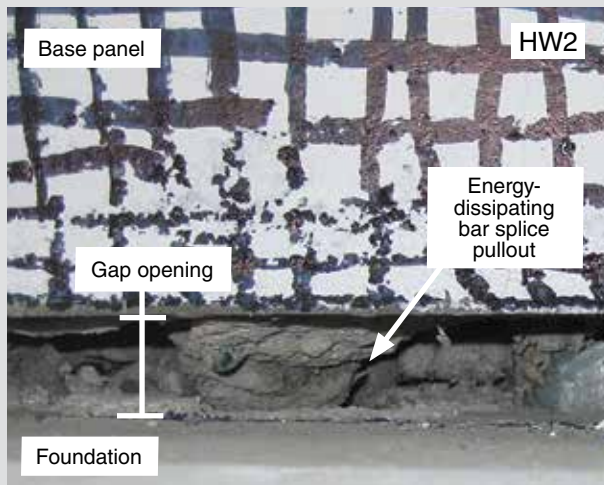
Figure 7. Energy-dissipating bar wrapped length.

of the structure (estimated as the coefficient for additional energy-dissipating bar debonding α_s times the bar diameter per ACI ITG-5.2). The coefficient α_s can be assumed equal to 0 and 2.0 at Δ_{wd} and Δ_{wm} , respectively. Concrete cores were taken through the thickness of the base panel around the end of the wrapped length of the energy-dissipating bars in two of the test specimens, supporting the use of α_s equal to 2.0 at Δ_{wm} . The wrapped length of the energy-dissipating bars (**Fig. 7**) should be designed such that the strains of the bars at Δ_{wm} are greater than $0.5\epsilon_{su}$ to ensure sufficient energy dissipation but do not exceed the maximum allowable strain of $0.85\epsilon_{su}$ (per ACI ITG-5.2) to prevent low-cycle fatigue fracture, where ϵ_{su} is the monotonic strain capacity of the steel at peak strength. Energy-dissipating bar strains up to $0.85\epsilon_{su}$ were used in the design of the test specimens (Table 1), with no bar fracture observed during the experiments. The wrapped length can be located in the bottom of the base panel or the top of the foundation. In either configuration, the energy-dissipating bars should also be isolated from the grout through the thickness of the grout pad at the base joint (that is, the wrapped length should include the thickness of the grout pad).

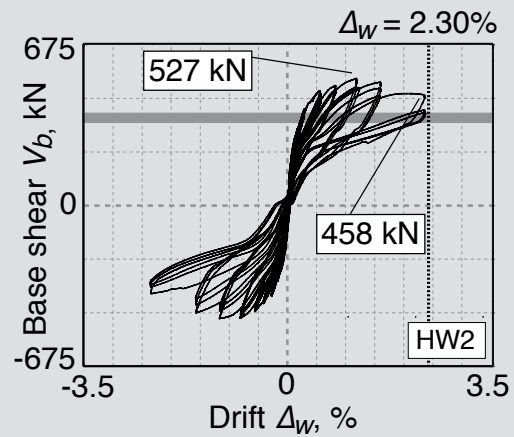
Sufficient development length or anchorage should be provided at both ends of the wrapped region of the energy-dissipating bars. Due to the large reversed-cyclic steel strains expected through Δ_{wm} , Type II grouted mechanical splices specified in section 21.1.6 of ACI 318-11 and permitted by section 5.4.2 of ACI ITG-5.2 should not be used for the energy-dissipating bars in hybrid precast concrete walls in seismic regions unless the splices have been tested and validated under cyclic loading up to a steel strain of at least $0.85\epsilon_{su}$. Pullout of the energy-dissipating bars from the foundation occurred in specimen HW2 due to the failure of the grout within Type II splice connectors prior to Δ_{wm} (**Fig. 8**). The pullout caused the energy-dissipating bar

elongations and strains to be smaller than designed, resulting in smaller lateral strength and energy dissipation of the wall (Fig. 3). Figure 8 shows the measured $V_b-\Delta_w$ behavior of specimen HW2, with the gray shaded band indicating the calculated strength of the wall (using the measured posttensioning steel forces, gravity load, and neutral axis length, as well as the ACI 318-11 and ACI ITG-5.2 concrete stress blocks) excluding the contribution of the energy-dissipating bars. Comparing this range with the measured strength, it was confirmed that specimen HW2 was essentially behaving as a fully posttensioned wall with no effective energy-dissipating steel reinforcement by the end of the test.

The grout used in the energy-dissipating bar splice connectors in specimen HW2 satisfied the splice manufacturer's specifications, and the splice itself satisfied the performance requirements in ACI 318-11 and *ACI 133: Acceptance Criteria for Mechanical Connector Systems for Steel Reinforcing Bars*¹⁵ for Type II mechanical connectors. However, the energy-dissipating bars in specimen HW2 were subjected to much greater strains and over a significantly larger number of cycles than required to classify a Type II connector per ACI 318-11 and AC133, causing the pullout of the bars. As a result, it is recommended that in validating Type II connectors for use in energy-dissipating bar splices of hybrid precast concrete shear walls, the bars should first be subjected to 20 loading cycles through $+0.95\epsilon_{sy}$ and $-0.5\epsilon_{sy}$, as required by AC133 (where ϵ_{sy} is the yield strain of the energy-dissipating steel). Beyond this point, six cycles should be applied at each load increment, with the compression strain amplitude kept constant at $-0.5\epsilon_{sy}$ and the tension strain amplitude increased to a value not less than 1.25 times and not more than 1.5 times the strain amplitude from the previous load increment. Testing should continue until the tension strain amplitude



Energy-dissipating bar splice pullout



V_b-Δ_w behavior

Figure 8. Performance of specimen HW2. Note: 1 kN = 0.225 kip.

reaches or exceeds +0.85ε_{su} (that is, the maximum allowable energy-dissipating bar strain per ACI ITG-5.2) over six cycles. These requirements would result in similar cyclic loading conditions during the validation testing of the splices as the loading conditions that can develop in the energy-dissipating bars during the validation testing of hybrid shear walls based on ACI ITG-5.1.

In lieu of Type II mechanical splices, the full development length of the energy-dissipating bars can be cast or grouted (during wall erection) into the base panel and the foundation. Both of these fully-developed connection techniques were successfully used in this project with no observed pullout of the bars from the concrete or grout.^{2,3}

Posttensioning steel strain limitation

The elongations of the posttensioning strands can also be found by assuming that the wall displaces like a rigid body rotating through the gap opening at the base joint (appendix).¹ The strain increment in each tendon due to the lateral displacements of the wall can then be calculated by dividing the strand elongations with the unbonded length. Significant nonlinear straining of the posttensioning steel should be prevented to limit the prestress losses at Δ_{wm}. Furthermore, the anchorage system for the posttensioning tendons should be capable of allowing the strands to reach the predicted stresses and total strains (that is, prestrain plus the strain increment due to gap opening) at Δ_{wm} without strand wire fracture or wire slip. Unless the posttensioning anchors have been qualified for greater strand strains under cyclic loading, the total strand strains (including prestrain) should be limited to a maximum allowable strain of 0.01. Strand wire fractures can occur if tendon strains exceed 0.01.¹⁶⁻¹⁸ With this strain limit, which was used in the design of the hybrid specimens tested as part of

this project, no strand wire fracture or slip was observed and the tendons remained mostly in the linear-elastic range through Δ_{wm}.

Wall restoring force

Hybrid precast concrete walls must maintain an adequate amount of restoring force (self-centering capability) to ensure that the gap at the base joint is fully closed upon removal of the lateral load after tensile yielding of the energy-dissipating bars. This restoring force, which comprises the gravity axial force and the total posttensioning force (including losses) at Δ_{wm}, should be sufficient to yield the tensile energy-dissipating bars back in compression and return them to essentially zero strain. Figure 9 demonstrates this requirement using an idealized stress-strain relationship for the energy-dissipating steel. As the wall is displaced from the initial unloaded position (close to point A), the energy-dissipating bars yield in tension (point B) and reach the maximum strain ε_{sm} (point C) at Δ_{wm}. Upon unloading of the wall, the restoring force must be able to yield the tensile energy-dissipating bars back in compression (point D) and return the bars to zero strain (point E), resulting in a total stress reversal of f_{sm} plus f_{sy} (where f_{sm} is the energy-dissipating steel stress at Δ_{wm}) such that no significant plastic tensile strains accumulate in the steel. The use of the full energy-dissipating bar stress reversal of f_{sm} plus f_{sy} in design means that the elastic restoring force provided by the energy-dissipating steel is conservatively ignored when determining the required wall restoring force.

For walls in which, for design purposes, the individual energy-dissipating bars can be combined (lumped) into a single steel area (equal to the sum of the individual bar areas) at the wall centerline (which requires that the bars

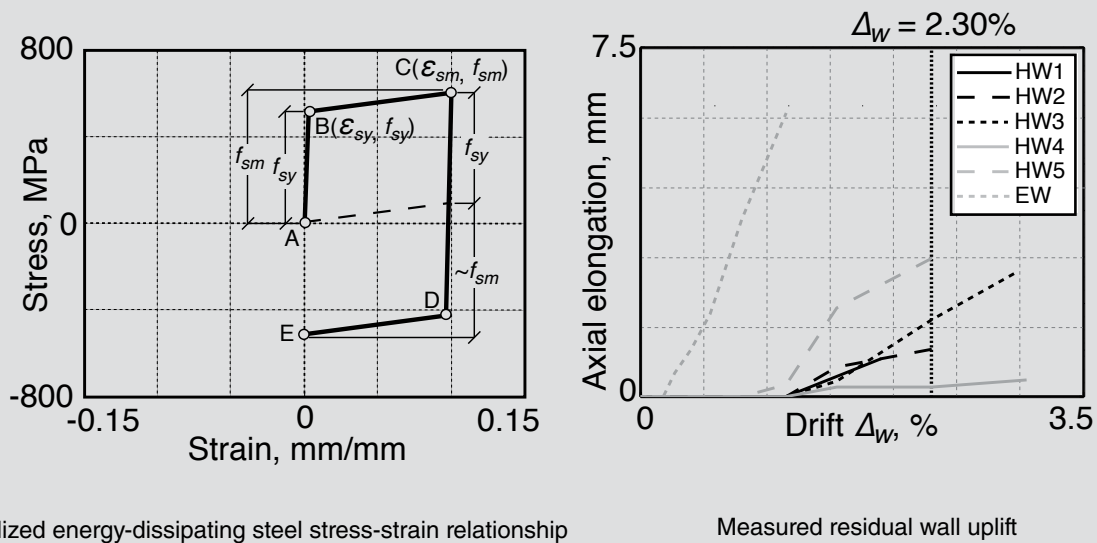


Figure 9. Restoring force. Note: f_{sm} = energy-dissipating steel stress at Δ_{wm} ; f_{sy} = yield strength of energy-dissipating steel; ϵ_{sm} = energy-dissipating steel strain at Δ_{wm} ; ϵ_{sy} = yield strain of energy-dissipating steel at f_{sy} . 1 mm = 0.0394 in.; 1 MPa = 0.145 ksi.

be placed near the centerline, similar to Fig. 1) and the posttensioning tendons on either side of the wall centerline can be combined into a single tension-side tendon area and a single compression-side tendon area, the design requirement for the restoring force can be written as Eq. (5).

$$A_p(f_{pm} - 0.5f_{p,loss}) + N_{wd} > A_s(f_{sm} + f_{sy}) \quad (5)$$

where

A_p = total posttensioning steel area (sum of the combined tension-side and compression-side tendon areas)

f_{pm} = predicted stress¹ in the combined tension-side posttensioning tendon under monotonic loading to Δ_{wm}

$f_{p,loss}$ = predicted stress loss¹ in the combined compression-side posttensioning tendon at Δ_{wm} due to nonlinear strand behavior associated with reversed-cyclic loading of the wall to $\pm\Delta_{wm}$

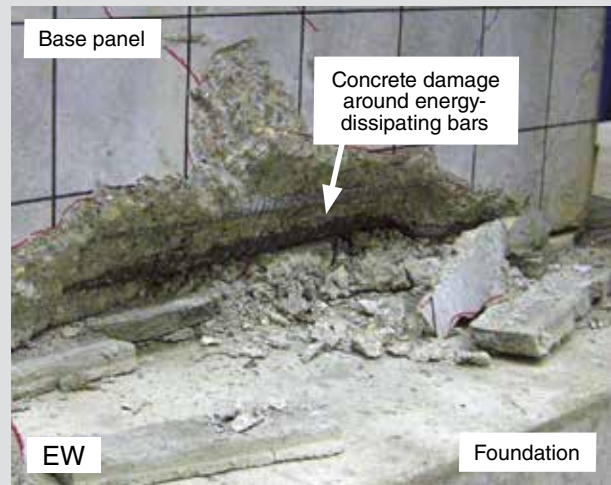
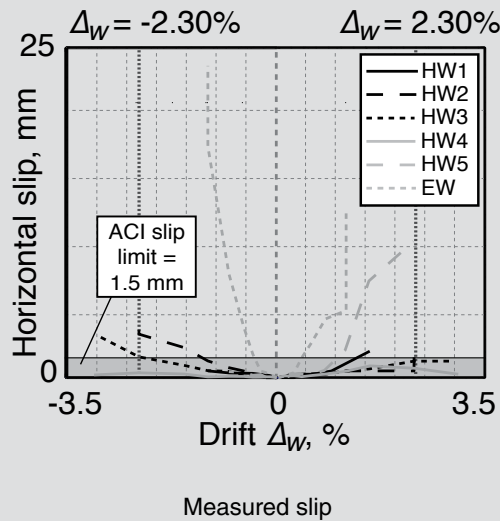
A_s = total combined energy-dissipating steel area

The application of Eq. (5) is demonstrated in the appendix design example. Where the posttensioning tendons or the energy-dissipating bars cannot be combined, Eq. (5) should be revised to separately consider the steel stress in each tendon or bar.

The design requirement given by Eq. (5) is more demanding than that given in section 5.3.1 of ACI ITG-5.2. The restoring force in specimens HW1, HW2, HW3, and HW4 satisfied Eq. (5), while the force in specimens HW5 and EW did not. To investigate the effect of the wall restoring force, Fig. 9 shows the residual axial elongation (that is,

heightening of the wall on unloading from a lateral displacement) at the centerline of each specimen (measured at the same elevation as the applied lateral load) on return of the wall to Δ_w of 0% from the third cycle in each drift series (where upward displacement is defined as positive). The accumulation of this residual axial elongation represents a reduction (that is, loss) or lack of sufficient axial restoring force in the system. In specimens HW1, HW2, HW3, and HW4, the axial elongation did not start to accumulate until the drift series with Δ_w of $\pm 1.55\%$, which coincided with the initiation of posttensioning stress losses. Among these four walls, the largest residual elongation occurred in specimen HW3, where the maximum elongation on unloading from Δ_w of $\pm 2.30\%$ was 1.7 mm (0.067 in.). This small uplift did not adversely affect the performance of the wall.

In comparison, the residual axial elongation in specimen HW5 started to accumulate earlier (during the drift series with Δ_w of $\pm 1.15\%$), and the maximum residual elongation at Δ_w of 2.30% was almost twice as large (3.0 mm [0.12 in.]). This increased uplift is related to the reduced self-centering force in the wall (from the posttensioning force plus the gravity load) and the increased contribution of the energy-dissipating steel to the total base moment strength (due to the use of a large κ_d in design [Table 1]). Specimen HW5 marginally satisfied the restoring force requirement in ACI ITG-5.2 but did not satisfy Eq. (5). Once the energy-dissipating bars yielded in tension, the restoring force was not sufficient to yield the bars back in compression and bring to essentially zero strain upon returning of the wall to Δ_w of 0%. Over successive loading/unloading cycles with increasing wall drift, the residual (plastic) tensile strains in the energy-dissipating bars resulted in the complete uplift of the structure at the base



Base panel damage in specimen EW

Figure 10. Horizontal slip along base joint. Note: 1 mm = 0.0394 in.

joint, overcoming the downward restoring force. This undesirable behavior ultimately caused out-of-plane displacements of the wall base during unloading and buckling of the energy-dissipating bars in compression (Fig. 4), leading to the rapid deterioration and failure of the wall.

Specimen EW accumulated significantly greater residual axial elongations compared with the hybrid walls, beginning from the drift series with Δ_w of $\pm 0.27\%$, with a maximum uplift of 6.1 mm (0.24 in.) after the last cycle to Δ_w of $\pm 1.15\%$. The large uplift of the emulative system was related to the lack of posttensioning steel, which resulted in an even smaller restoring force (provided only by the gravity load) than in specimen HW5. The residual elongations of specimen EW accumulated rapidly, leading to the failure of the wall due to excessive horizontal in-plane shear slip at the base joint and localized splitting of the base panel concrete around the energy-dissipating bars (Fig. 10), with larger strength and stiffness degradation than in specimen HW5.³

Shear design across horizontal joints

To prevent significant horizontal slip of the wall during loading up to Δ_{wm} , the shear friction strength at the horizontal joints should be greater than the joint shear force demand. The joint shear forces should be calculated from the maximum wall base shear force V_{wm} corresponding to the probable base moment strength M_{wm} of the wall at Δ_{wm} (appendix). The nominal shear friction strength at the base joint can be determined as the assumed shear friction coefficient μ_{ss} of 0.5 multiplied by the calculated compression force in the contact region at the wall toe. For the upper panel-to-panel joints, μ_{ss} can be taken as 0.6, and the shear friction design method in section 11.6 of ACI 318-11 can be used by combining the shear friction strength provided by

the axial force (from the posttensioning steel and the gravity load) with the shear friction strength from the yielding of the mild steel bars crossing the upper joint at both ends (Fig. 1). As recommended in section 5.5.3 of ACI ITG-5.2, a smaller value of μ_{ss} is assumed at the base joint due to the expected deterioration of the concrete and grout pad at Δ_{wm} , leading to a smaller shear friction strength compared with the upper joints.

The specimens tested as part of this project were designed using this approach. The horizontal shear slip at the upper panel-to-panel joint of the walls was negligible. Figure 9 shows the measured slip at the centerline of the base joint from the six specimens. For each specimen, only the peak of the third cycle in each drift series was plotted, except for the final drift series where the peaks from all cycles were plotted. For walls that satisfied the axial restoring force requirement described previously in this paper (specimens HW1, HW2, HW3, and HW4), only a small amount of shear slip occurred along the base joint. In some instances, the measured base slip of these specimens exceeded the maximum allowable slip of 1.5 mm (0.06 in.) per section 7.1.4(3) of ACI ITG-5.1. However, this amount of base slip did not adversely affect the performance of the walls, indicating that the current allowable slip limit of 1.5 mm (0.06 in.) in ACI ITG-5.1 may be too conservative. A more reasonable allowable slip limit may be 3.8 mm (0.15 in.), which was the largest measured base slip among the specimens whose performance was not affected by slip (that is, specimens HW1, HW2, HW3, and HW4).

Specimens HW5 and EW did not satisfy the axial restoring force requirement described previously in this paper, resulting in excessive in-plane slip at the base joint. Under load reversals with increasing in-plane slip, significant out-of-plane displacements also developed at the base of specimen HW5 (Fig. 4), resulting in the buckling of the



energy-dissipating bars in compression (Fig. 4). Unlike specimen HW5, no significant out-of-plane displacements occurred in specimen EW. Instead, the concrete around the energy-dissipating bars deteriorated due to the shear force transfer from the bars to the surrounding concrete, ultimately causing failure through the splitting of the base panel concrete (Fig. 9).

Other wall panel reinforcement

The other wall panel reinforcement, not continuous across the horizontal joints, includes shear (that is, diagonal-tension) reinforcement, edge reinforcement, reinforcement to control temperature and shrinkage cracks, and reinforcement to support panel lifting inserts. The base panel is expected to develop diagonal cracking; thus, distributed vertical and horizontal steel reinforcement should be designed according to the shear requirements in ACI 318-11, specifically the applicable requirements in sections 21.9.2 and 21.9.4. The specimens tested as part of this project satisfied these requirements and developed well-distributed hairline cracking in the base panel (Fig. 5). The cracks visible in the photographs were highlighted with markers during each test for enhanced viewing. The upper panels of the solid walls developed no cracking; thus, the distributed reinforcement in these panels can be reduced to satisfy the requirements in section 16.4.2 of ACI 318-11. In perforated walls, the reinforcement in both the base and upper panels includes additional mild steel bars for the panel chords around the perforations. The design of this panel chord reinforcement using a simplified finite element analysis of the wall through Δ_{wm} is described in Smith and Kurama.¹

Section 21.9.6.4(e) of ACI 318-11 should be satisfied for the termination and development of the base panel horizontal distributed reinforcement within the confined boundary regions at the wall toes. The horizontal bars in specimens HW1, HW2, and HW3 were not developed inside the boundary regions (Fig. 6), reducing the effectiveness of these bars. During the larger drift cycles after concrete cover spalling at the wall toes, the ends of the horizontal distributed bars near the base were exposed, causing the bars to delaminate and, subsequently, the cover spalling to extend farther along the length of the wall (Fig. 6). When the horizontal bars were terminated inside the confinement hoop cages (which was done in specimens HW4 and HW5), no bar delamination was observed and the concrete cover spalling did not extend beyond the wall toes (Fig. 6).

In addition to the distributed steel, reinforcement should be placed around the entire exterior perimeter of each wall panel using mild steel bars placed parallel to each panel edge. As required by section 4.4.10 of ACI ITG-5.2, the mild steel reinforcement along the bottom edge of the base panel (appendix) should provide a nominal tensile strength of not less than 87.6 kN/m (6 kip/ft) along the length of the panel. The objective of this reinforcement is to limit the

vertical concrete cracks initiating from the bottom of the base panel near the tip of the gap (that is, near the neutral axis).¹⁹ Thus, the bars should be placed as close to the bottom of the panel as practically possible while also satisfying the ACI 318-11 concrete cover and spacing requirements. The bottom edge bars in the base panel should be anchored using a standard 90° hook at the wall toes with sufficient development length from the critical location at the neutral axis (that is, at a distance c_m from each end of the wall). The bottom edge reinforcement in the wall specimens tested as part of this project was designed using this approach. Strain gauges placed on the bars near the critical location indicated strains reaching approximately $0.85\varepsilon_{sy}$ at Δ_{wm} , supporting the design requirement.

Flexural design of upper joints

The energy-dissipating bars crossing the base joint do not continue into the upper panel-to-panel joints (Fig. 1), resulting in a significant reduction in the lateral strength of the wall at these locations. The philosophy behind the flexural design of the upper panel-to-panel joints is to prevent significant gap opening and nonlinear material behavior during lateral displacements up to the maximum-level wall drift Δ_{wm} . Except for the base joint, where the wall is designed to rotate about the foundation, the structure should behave essentially as a rigid body through Δ_{wm} . Thus, the design of the upper panel-to-panel joints is conducted for the maximum joint moment demands corresponding to the probable base moment strength M_{wm} of the wall.¹

To prevent significant gap opening at the upper panel-to-panel joints, mild steel reinforcement crossing these joints should be designed at the panel ends and placed in a symmetrical layout (Fig. 1). As shown in the appendix, the design of this reinforcement is based on the principles of equilibrium, linear material models, and a linear strain distribution (that is, plane sections remain plane assumption). The design requires that the tension steel strain be limited to ε_{sy} to limit gap opening and the maximum concrete compressive stress be limited to $0.5f'_c$ to keep the concrete linear elastic (where f'_c is the compressive strength of the unconfined panel concrete). These material limits were used in the design of the wall specimens tested as part of this project with no undesirable behavior developing in the upper joints.²⁻⁴ To prevent strain concentrations in the upper panel-to-panel joint steel, a short prescribed length of the bars (approximately 100 to 150 mm [4 to 6 in.] long) should be unbonded (wrapped in a plastic sleeve) at each joint.

Conclusion

This paper describes the key aspects of a performance-based design approach, including a design example, for special unbonded posttensioned hybrid precast concrete shear walls in seismic regions. The proposed design



guidelines were developed and validated using the measured behaviors from six 0.4-scale multi-panel wall test specimens (four solid and two perforated walls) subjected to service-level gravity loads combined with reversed-cyclic lateral loading. It is concluded that hybrid precast concrete walls can satisfy all requirements for special reinforced concrete shear walls in high seismic regions with improved performance; however, critical design, detailing, and analysis considerations need to be undertaken to avoid undesirable failure mechanisms such as anchorage failure of the energy-dissipating bars, permanent uplift and excessive slip of the wall at the base joint, and premature crushing of the confined concrete at the wall toes. Ultimately, the recommendations in this paper are aimed at allowing practicing engineers and precast concrete producers to design ACI-compliant special hybrid shear walls with predictable, reliable, and improved seismic performance.

Acknowledgments

This research was funded by the Charles Pankow Foundation and PCI. Additional technical and financial support was provided by the High Concrete Group LLC, the Consulting Engineers Group Inc., and the University of Notre Dame. The authors acknowledge the support of the PCI Research and Development Committee, the PCI Central Region, and the members of the project advisory panel, who include Walt Korkosz (chair) of the Consulting Engineers Group Inc., Ken Baur of the High Concrete Group LLC, Neil Hawkins of the University of Illinois at Urbana-Champaign, S. K. Ghosh of S. K. Ghosh Associates Inc., and Dave Dieter of Mid-State Precast LP. The authors also thank Professor Michael McGinnis and undergraduate student Michael Lisk from the University of Texas at Tyler for monitoring the response of the test specimens using three-dimensional digital image correlation. Additional assistance and material donations were provided by Brian Balentine of Builders Iron Works Inc., Jenny Bass of Essve Tech Inc., Randy Draginis and Norris Hayes of Hayes Industries Ltd., Randy Ernest of Prestress Supply Inc., Eric Fries of Contractors Materials Co., Rod Fuss of Ambassador Steel Corp., Tony Johnson of the Concrete Reinforcing Steel Institute, Martin Koch of Southwestern Supplies Inc., Chris Lagaden of Ecco Manufacturing, Stan Landry of Enerpac Precision SURE-LOCK, Richard Lutz of Summit Engineered Products, Kristen Murphy of Acument Global Technologies, Shane Whitacre of Dayton Superior Corp., Phil Wiedemann of PCI Central Region, and Steve Yoshida of Sumiden Wire Products Corp. The authors thank these individuals, institutions, and companies for supporting the project. The opinions, findings, conclusions, and recommendations expressed in this paper are those of the authors and do not necessarily represent the views of the individuals and organizations acknowledged.

References

1. Smith, B., and Y. Kurama. 2012. *Seismic Design Guidelines for Special Hybrid Precast Concrete Shear Walls*. Research report NDSE-2012-02. Notre Dame, IN: University of Notre Dame. hybridwalls.nd.edu/Project/Downloads/Design_Guidelines.pdf.
2. Smith, B., Y. Kurama, and M. McGinnis. 2013. "Behavior of Precast Concrete Shear Walls for Seismic Regions: Comparison of Hybrid and Emulative Specimens." *Journal of Structural Engineering* 139 (11): 1917–1927. ascelibrary.org/doi/abs/10.1061/%28ASCE%29ST.1943-541X.0000755.
3. Smith, B., Y. Kurama, and M. McGinnis. 2012. *Hybrid Precast Wall Systems for Seismic Regions*. Research report NDSE-2012-01. Notre Dame, IN: University of Notre Dame. hybridwalls.nd.edu/Project/Downloads/Final_Report.pdf.
4. Smith, B., Y. Kurama, and M. McGinnis. 2011. "Design and Measured Behavior of a Hybrid Precast Concrete Wall Specimen for Seismic Regions." *Journal of Structural Engineering* 137 (10): 1052–1062.
5. ACI (American Concrete Institute) Committee 318. 2011. *Building Code Requirements for Structural Concrete (ACI 318-11) and Commentary (ACI 318R-11)*. Farmington Hills, MI: ACI.
6. ACI Innovation Task Group 5. 2007. *Acceptance Criteria for Special Unbonded Post-Tensioned Precast Structural Walls Based on Validation Testing and Commentary*. ACI ITG-5.1. Farmington Hills, MI: ACI.
7. ACI Innovation Task Group 5. 2009. *Requirements for Design of a Special Unbonded Post-Tensioned Precast Shear Wall Satisfying ACI ITG-5.1 (ACI ITG-5.2-9) and Commentary*. Farmington Hills, MI: ACI.
8. ASCE (American Society of Civil Engineers) and SEI (Structural Engineering Institute). 2010. *Minimum Design Loads for Buildings and Other Structures*. ASCE/SEI 7-10. Reston, VA: ASCE and SEI.
9. Farrow, K., and Y. Kurama. 2003. "SDOF Demand Index Relationships for Performance-Based Seismic Design." *Earthquake Spectra* 19 (4): 799–838.
10. Seo, C., and R. Sause. 2005. "Ductility Demands on Self-Centering Systems under Earthquake Loading." *ACI Structural Journal* 102 (2): 275–285.
11. Smith, B. 2013. "Design, Analysis, and Experimental Evaluation of Hybrid Precast Concrete Shear Walls



for Seismic Regions.” Doctoral diss. Notre Dame, IN: University of Notre Dame. etd.nd.edu/ETD-db/theses/available/etd-12132012-112729/unrestricted/Smith-BJ122012D.pdf.

12. Smith, B., and Y. Kurama. 2013. “Seismic Displacement Demands for Hybrid Precast Concrete Shear Walls.” In *ASCE Structures Congress: Bridging Your Passion with Your Profession*. Pittsburgh, PA, May 2–4. Reston, VA: ASCE.
13. Kurama, Y. 2005. “Seismic Design of Partially Post-Tensioned Precast Concrete Walls.” *PCI Journal* 50 (4): 100–125.
14. ICBO (International Conference of Building Officials). 1997. *Uniform Building Code, Volume 2: Structural Engineering Design Provisions*. Whittier, CA: ICBO
15. ICC (International Code Council). 2010. *AC133: Acceptance Criteria for Mechanical Connector Systems for Steel Reinforcing Bars*. Whittier, CA: ICC Evaluation Services.
16. Walsh, K., and Y. Kurama. 2010. “Behavior of Unbonded Post-tensioning Monostrand Anchorage Systems under Monotonic Tensile Loading.” *PCI Journal* 55 (1): 97–117.
17. Walsh, K., and Y. Kurama. 2012. “Effects of Loading Conditions on the Behavior of Unbonded Post-tensioning Strand-Anchorage Systems.” *PCI Journal* 57 (1): 76–96.
18. Kurama, Y., B. Weldon, and Q. Shen. 2006. “Experimental Evaluation of Posttensioned Hybrid Coupled Wall Subassemblages.” *Journal of Structural Engineering* 132 (7): 1017–1029.
19. Allen, M., and Y. Kurama. 2002. “Design of Rectangular Openings in Precast Walls under Combined Vertical and Lateral Loads.” *PCI Journal* 47 (2): 58–83.

Notation

A_{gross} = gross area of wall cross section (taken at section with perforations in case of perforated walls)

A_p = total posttensioning steel area

A_s = total energy-dissipating steel area

A_{sh} = effective shear area of wall cross section

c_m = neutral axis length at base joint at Δ_{wm}

C_d = ASCE 7-10 deflection amplification factor

e_p = distance of tension-side and compression-side post-tensioning tendons from wall centerline

e_s = distance of tension-side and compression-side energy-dissipating bars from wall centerline

f'_c = compressive strength of unconfined panel concrete

f_{pd} = posttensioning steel stress at Δ_{wd}

f_{pi} = initial stress of posttensioning steel after all short-term and long-term losses but before any lateral displacement of wall

$f_{p,loss}$ = stress loss in compression-side posttensioning tendon at Δ_{wm} due to nonlinear material behavior associated with reversed-cyclic loading of wall to $\pm \Delta_{wm}$

f_{pm} = posttensioning steel stress at Δ_{wm}

f_{pu} = ultimate strength of posttensioning steel

f_{sd} = energy-dissipating steel stress at Δ_{wd}

f_{sm} = energy-dissipating steel stress at Δ_{wm}

f_{su} = ultimate (maximum) strength of energy-dissipating or other mild steel

f_{sy} = yield strength of energy-dissipating steel or other mild steel

h_p = plastic hinge height over which plastic curvature is assumed to be uniformly distributed at wall base

H_w = wall height from top of foundation

I_e = reduced linear-elastic effective moment of inertia of wall cross section

I_{gross} = moment of inertia of gross wall cross section (taken at section with perforations in case of perforated walls)

l_h = confined region length at wall toes (center-to-center of bars)

l_{hoop} = length of individual confinement hoop (center-to-center of bars)

L_w = wall length

M_{wd} = wall design base moment at Δ_{wd}

M_{wm} = probable base moment strength of wall at Δ_{wm}

M_{wn} = contribution of wall gravity axial force N_{wd} to sat-



- isfy M_{wd}
- M_{wp} = contribution of posttensioning steel to satisfy M_{wd}
- M_{ws} = contribution of energy-dissipating steel to satisfy M_{wd}
- N_{wd} = actored design gravity axial force at wall base for design load combination being considered
- R = ASCE 7-10 response modification factor
- s_{bot} = first confinement hoop distance from bottom of base panel to center of bar
- s_{hoop} = confinement hoop spacing (center-to-center of bars)
- V_b = wall base shear force
- V_{wd} = design wall base shear force corresponding to M_{wd} at Δ_{wd}
- V_{wm} = maximum wall base shear force corresponding to M_{wm} at Δ_{wm}
- w_{hoop} = width of individual confinement hoop (center-to-center of bars)
- α_s = ACI ITG-5.2 coefficient to estimate additional energy-dissipating bar debonding that is expected to occur during reversed-cyclic lateral displacements of wall
- β = relative energy dissipation ratio per ACI ITG-5.1⁶
- β_{min} = minimum required relative energy dissipation ratio per ACI ITG-5.1
- Δ_w = wall drift, defined as relative lateral displacement at wall top divided by height from top of foundation
- Δ_{wc} = validation-level wall drift based on ACI ITG-5.1
- Δ_{wd} = design-level wall drift corresponding to design-basis earthquake
- Δ_{we} = linear-elastic wall drift under V_{wd}
- Δ_{wm} = maximum-level wall drift corresponding to maximum-considered earthquake
- ϵ_{sm} = energy-dissipating steel strain at Δ_{wm}
- ϵ_{su} = strain of energy-dissipating steel or other mild steel at f_{su}
- ϵ_{sy} = yield strain of energy-dissipating steel or other mild steel at f_{sy}
- κ_d = energy-dissipating steel moment ratio, defining relative amounts of energy-dissipating resistance from $A_s f_{sd}$ and restoring resistance from $A_p f_{pd}$ and N_{wd} at wall base
- μ_{ss} = coefficient of shear friction at horizontal joints



About the authors



Brian J. Smith, PhD, PE, is an assistant teaching professor in the Department of Civil and Environmental Engineering and Earth Sciences at the University of Notre Dame in Notre Dame, Ind.



Yahya C. Kurama, PhD, PE, is a professor in the Department of Civil and Environmental Engineering and Earth Sciences at the University of Notre Dame.

Abstract

This paper presents recommended seismic design and detailing guidelines for special unbonded posttensioned “hybrid” precast concrete shear walls, including a full-scale worked design example and supporting experimental evidence from six 0.4-scale test specimens. Hybrid precast concrete walls use a combination of mild steel bars (Grade 400 [Grade 60]) and high-strength unbonded posttensioning steel strands for lateral resistance across horizontal joints. The mild steel bars are designed to yield in tension and com-

pression, providing energy dissipation. The unbonded posttensioning strands provide self-centering capability to reduce the residual lateral displacements of the structure after a large earthquake. The proposed design guidelines are aimed to allow practicing engineers and precast concrete producers to design American Concrete Institute–compliant hybrid shear walls with predictable and reliable seismic behavior. Ultimately, the results from this project support the U.S. code approval of the hybrid precast concrete wall system as a special reinforced concrete shear wall for moderate and high seismic regions.

Keywords

Hybrid, joint, posttensioned, seismic, shear wall, testing.

Review policy

This paper was reviewed in accordance with the Precast/Prestressed Concrete Institute’s peer-review process.

Reader comments

Please address any reader comments to journal@pci.org or Precast/Prestressed Concrete Institute, c/o *PCI Journal*, 200 W. Adams St., Suite 2100, Chicago, IL 60606. ¶